Ring-Opening Vibrations of Spherosiloxanes

Peter Bornhauser and Gion Calzaferri*

Institute for Inorganic and Physical Chemistry, University of Berne, Freiestrasse 3, CH-3000 Bern 9, Switzerland

The ring-opening vibrations of the spherosilasesquioxanes of the general formula $(HSiO_{3/2})_{2n}$, $n = 2, 3, 4$, etc., are normal modes in which all Si−O stretching and/or O−Si−O bending displacements of the considered ring are in phase. We have investigated the vibrational structure of the experimentally well-known $H_8Si_8O_{12}$ and $H_{10}Si_{10}O_{15}$ and of I_h-$H_{20}Si_{20}O_{30}$ and O_h-$H_{24}Si_{24}O_{36}$, which are not yet known as isolated molecules. The energy range of the 11 IR active, the 15 Raman active, and the three inactive ring-opening modes which belong to the 4-, 5-, and 6-ring vibrations of O_h-$H_8Si_8O_{12}$, D_{5h}-$H_{10}Si_{10}O_{15}$, I_h-$H_{20}Si_{20}O_{30}$, and O_h-$H_{24}Si_{24}O_{36}$ decreases from 490−390 to 440−250 to 340−219 cm^{-1}. The 4-, 5-, and 6-rings are in fact built of four, five, and six Si atoms plus four, five, and six O atoms, respectively. The totally symmetric vibrations show predominantly stretching character with one exception, the δ(O−Si−O) line at 451 cm^{-1} of $H_{24}Si_{24}O_{36}$. They occur in specific regions, namely, at 460−440 cm^{-1} for the 4-ring, at 340−250 cm^{-1} for the 5-ring, and at 220−210 cm^{-1} for the 6-ring. We show that the ring-opening vibrations of the hydrosilasesquioxanes suggest a new way to study the pore-opening vibrations of zeolites, which simplifies the problem remarkably and thus leads to a better understanding of the more complex extended structures. The vibrations of the investigated spherosiloxanes can be divided into six distinct regions denoted as ν(Si−H), ν_{as}(Si−O−Si), δ(O−Si−H), ν_s(Si−O−Si), δ(O−Si−O), and δ(Si−O−Si). This means that the concept of group frequencies makes sense. However 10 modes were observed which do not fit into this general scheme, namely, the modes at 481 and 446 cm^{-1} ($H_8Si_8O_{12}$), at 455, 450, and 334 cm^{-1} ($H_{10}Si_{10}O_{15}$), at 336, 284, and 251 cm^{-1} ($H_{20}Si_{20}O_{30}$), and at 219 and 214 cm^{-1} ($H_{24}Si_{24}O_{36}$). All of them can be identified as ring-opening vibrations.

I. Introduction

The cage-shaped hydrosilasesquioxanes of the general formula $(HSiO_{3/2})_{2n}$, $n = 2, 3$, etc., are appealing molecules for studying structural, electronic, and vibrational properties of silicon dioxide cage structures. Some of them may be considered as molecular models of the building units found in infinitely extended zeolite and silicate frameworks. The crystal structures of $H_8Si_8O_{12}$,[1−3] $H_{10}Si_{10}O_{15}$,[4] and $H_{12}Si_{12}O_{18}$[5] were studied in detail, and those of the two isomers of $H_{14}Si_{14}O_{21}$[6] were reported. These molecules have recently been discussed as precursors for atomic scale control of the Si/SiO$_2$ interface.[7] $H_8Si_8O_{12}$ has shown to be a suitable starting molecule to synthesize mono[8] and higher[9] substituted octanuclear silasesquioxanes. Its electronic structure and the Si−H + Y−Z → Si−Y + H−Z reaction mechanism under retention of the cage have been studied.[10] Some of the $R_8Si_8O_{12}$ molecules have been discussed as building blocks for the preparation of highly silicic materials or as starting molecules for new organosiliceous materials.[11] Amazingly, stable encapsulation of atomic hydrogen upon γ-irradiation of $[(CH_3)_3SiO]_8Si_8O_{12}$ was reported recently.[12]

We measured and analyzed the IR, the FT-Raman, and the INS spectra of $H_8Si_8O_{12}$ in detail,[13−15] and the correlation between idealized D_{nh} oligomeric $(HSiO_{3/2})_{2n}$ ($n = 3, 4, 5$, and 6) was reported in a preliminary communication.[16] It was shown that the force field determined for $H_8Si_8O_{12}$ is appropriate to describe the fundamentals of $H_{10}Si_{10}O_{15}$. When carrying out this work, we observed that these molecules are suited as models for studying pore-opening vibrations, which are believed to play an important role in the dynamics and the transport properties

SCHEME 1: $H_8Si_8O_{12}$ (top left), $H_{10}Si_{10}O_{15}$ (top right), $H_{20}Si_{20}O_{30}$ (bottom left), and $H_{24}Si_{24}O_{36}$ (bottom right) in the Polyhedral Representation
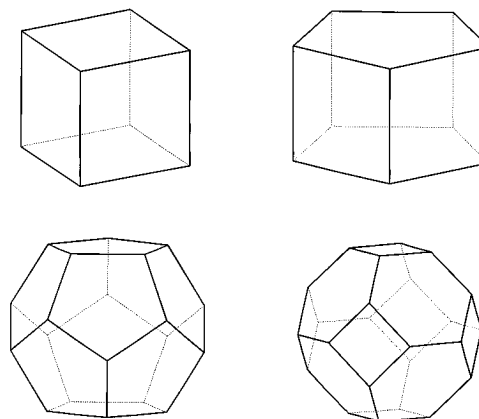
of zeolites. We explain this for O_h-$H_8Si_8O_{12}$, D_{5h}-$H_{10}Si_{10}O_{15}$, I_h-$H_{20}Si_{20}O_{30}$, and O_h-$H_{24}Si_{24}O_{36}$. Their geometry is illustrated in Scheme 1. The corners represent the positions of the Si atoms, while the bridging oxygen and the terminal hydrogen atoms are not shown. I_h-$H_{20}Si_{20}O_{30}$ and O_h-$H_{24}Si_{24}O_{36}$ are not yet known as isolated molecules. We introduce the ring-opening vibrations as normal modes in which all Si−O stretching and/or O−Si−O bending displacements of the considered ring are in phase, and we analyze their properties for the 4-, 5-, and 6-rings, which in fact are built of four, five, and six Si atoms plus four, five, and six O atoms, respectively.

The aluminosilicate framework of zeolite A can be built of double 4-rings (D4R) connected by oxygen bridges.[17] A detailed comparison between silasesquioxane molecules and LTA zeolites was presented recently.[18] We described $H_8Si_8O_{12}$

---

* Author to whom correspondence should be addressed.

SCHEME 2: Relation between the Structure of Zeolite A and $H_8Si_8O_{12}$ (right) and $H_{24}Si_{24}O_{36}$ (left)
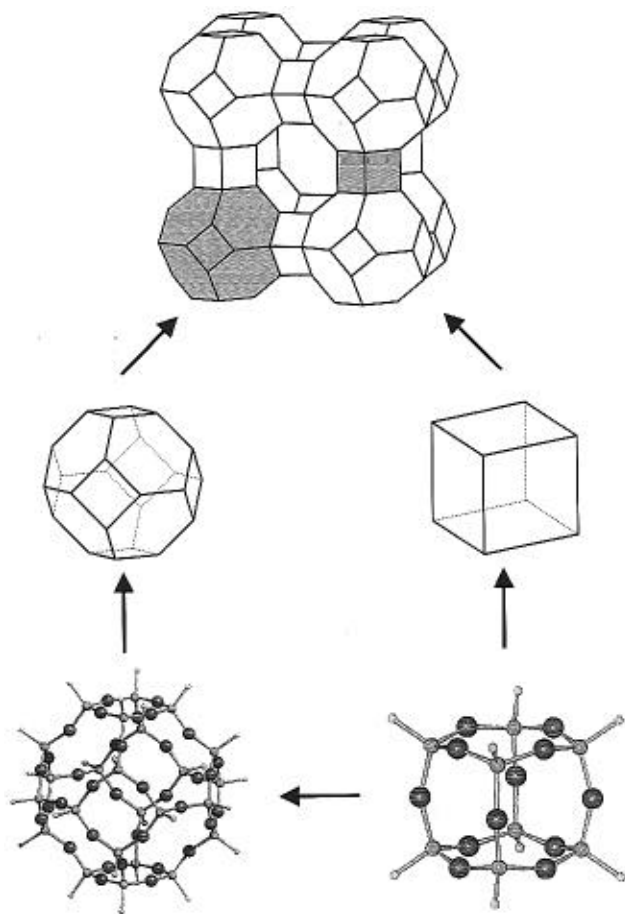
as a model for the vibrational structure of zeolite A.[14] A consequence of these ideas is shown in Scheme 2, in which the hydrosilasesquioxanes $H_8Si_8O_{12}$ and $H_{24}Si_{24}O_{36}$ are related to the structure of zeolite A. Since $H_{24}Si_{24}O_{36}$ bears the structure of the sodalite cage, it may be used as a link to the many zeolites in which this structure is present.[19] A similar link to clathrasils[20] can be tried via the $H_{20}Si_{20}O_{30}$. Several attempts have been made to assign the observed vibrational modes to specific local structural features of zeolites and especially to pore-opening vibrations.[21-27] We now show that the ring-opening vibrations of the hydrosilasesquioxanes suggest a new way to study the pore-opening vibrations of zeolites. This approach simplifies the problem remarkably and thus leads to a better understanding of the more complex extended structures.

II. Experimental Section

The normal mode calculations were performed by the Wilson GF matrix method[28] using the computer program package QCMP067.[29] The point charge model for describing molecular dipole moments was used to calculate relative infrared intensities. The atom charges, Si = +0.498, O = −0.305, and H = −0.040, were obtained from an extended-Hückel molecular orbital calculation[30] of $H_8Si_8O_{12}$ with the parameters reported in ref 8b. The bands of the calculated IR spectra were generated using a 1:1 mixture of a Lorentzian and a Gaussian curve which were adapted to the experimental bandwidths. The structure and the definition of the internal coordinates of the $(HSiO_{3/2})_{2n}$ ($n = 4, 5, 10,$ and 12) are illustrated in Schemes 3S and 4S. For details we refer to ref 14. This definition of the internal coordinates is consistent with the usual conventions. It is applicable to all spherosiloxanes and results in 24 Si−H and

TABLE 1: Bond Lengths (Å) and Bond Angles (deg) Used for $H_8Si_8O_{12}$ and $H_{10}Si_{10}O_{15}$

internal coordinate	$H_8Si_8O_{12}$	$H_{10}Si_{10}O_{15}$
R(Si−H)	1.48	1.48
r(Si−O)	1.62	1.61
s(Si−O)		1.60
α(O−Si−H)	109.5	109.5
β(O−Si−O)	109.5	109.5
γ(O−Si−H)		109.5
δ(O−Si−O)		109.5
Φ(Si−O−Si)	148.4	150.5
Ψ(Si−O−Si)		156.1

72 Si−O bond-stretching and in 72 O−Si−H, 72 O−Si−O, and 36 Si−O−Si valence angle bending coordinates for $H_{24}Si_{24}O_{36}$ with **F** and **G** matrices of dimension 276. The corresponding dimension of the **F** and **G** matrices for $H_{20}Si_{20}O_{30}$ is 230. The bond lengths and bond angles of O_h-$H_8Si_8O_{12}$ and of D_{5h}-$H_{10}Si_{10}O_{15}$ used in this study are reported in Table 1.

The vibrational analysis of all $(HSiO_{3/2})_{2n}$ oligomers was performed using the modified general valence force field determined for $H_8Si_8O_{12}$.[14] According to Table 5 of ref 14, not all internal force constants are linearly independent because of symmetry. Three of the 13 off-diagonal elements must therefore be eliminated. We have done this by setting $f_{\alpha\alpha}$, $f_{\beta\beta}$, and $f'_{r\alpha}$ equal to 0 when carrying out the calculations. This arbitrary choice does not influence any of our results. The molecules $H_8Si_8O_{12}$, $D_8Si_8O_{12}$, $H_{10}Si_{10}O_{15}$, and $D_{10}Si_{10}O_{15}$ were prepared and purified as described in refs 9e and 31−33, and their IR and Raman spectra were measured as described in refs 14, 33, and 34.

III. Correlation of the Vibrational Spectra of $H_8Si_8O_{12}$ and $H_{10}Si_{10}O_{15}$

Structure and Irreducible Representations. $H_8Si_8O_{12}$ and $H_{10}Si_{10}O_{15}$ single crystals show S_6 and C_2 molecular symmetry, respectively.[2-4] The deviation from the "ideal" O_h and D_{5h} symmetry is small, and spectra measured in solution are fully compatible with O_h and D_{5h} symmetry, respectively. It is therefore convenient and useful to describe the vibrations of these molecules within the O_h and the D_{5h} point groups, respectively, and to discuss deviations of this symmetry separately; see refs 13−15. On this basis the 78 vibrational degrees of freedom of $H_8Si_8O_{12}$ and the 99 ones of $H_{10}Si_{10}O_{15}$ are divided among the irreducible representations as follows (R = Raman active, IR = infrared active, in = inactive).

O_h-$H_8Si_8O_{12}$:

$$\Gamma_{vib} = 3A_{1g}(R) + A_{2g}(in) + 4E_g(R) + 3T_{1g}(in) + $$
$$6T_{2g}(R) + 3A_{2u}(in) + 3E_u(in) + 6T_{1u}(IR) + 4T_{2u}(in) \quad (1)$$

D_{5h}-$H_{10}Si_{10}O_{15}$:

$$\Gamma_{vib} = 7A_1'(R) + 3A_2'(in) + 10E_1'(IR) + 11E_2'(R) + $$
$$3A_1''(in) + 6A_2''(IR) + 9E_1''(R) + 10E_2''(in) \quad (2)$$

From this follows that the IR spectrum of O_h-$H_8Si_8O_{12}$ consists of six and that of D_{5h}-$H_{10}Si_{10}O_{15}$ of 16 fundamentals. The Raman spectrum of O_h-$H_8Si_8O_{12}$ consists of 13 fundamentals, whereas 27 lines are expected for D_{5h}-$H_{10}Si_{10}O_{15}$.

D_{nh}-$D_{(n+1)h}$ **Correlation.** We consider the members of the oligomeric $(HSiO_{3/2})_{2n}$ molecules as a series of double-ring units with D_{nh} symmetry. This is illustrated in Figure 1. Since D_{4h} is a subgroup of the O_h point group, we apply a small distortion to the O_h-$H_8Si_8O_{12}$ so that it fits into this series. The correlation

Ring-Opening Vibrations of Spherosiloxanes

J. Phys. Chem., Vol. 100, No. 6, 1996 **2037**
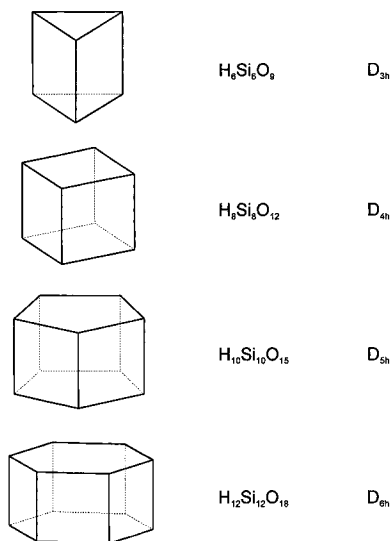
Figure 1. Oligomeric $(HSiO_{3/2})_{2n}$ ($n = 3, 4, 5,$ and 6) spherosiloxanes in the polyhedral representation as double-ring units.

for this symmetry lowering is straightforward.[35] The irreducible representations for the fundamentals of the four structures are as follows:

$$\Gamma_{T_6^H}^{D_{3h}} = 7A_1' + 3A_2' + 10E' + 3A_1'' + 6A_2'' + 9E''$$

$$\Gamma_{T_8^H}^{D_{4h}} = 7A_{1g} + 3A_{2g} + 5B_{1g} + 6B_{2g} + 9E_g + 3A_{1u} + \\ 6A_{2u} + 6B_{1u} + 4B_{2u} + 10E_u$$

$$\Gamma_{T_{10}^H}^{D_{5h}} = 7A_1' + 3A_2' + 10E_1' + 11E_2' + 3A_1'' + 6A_2'' + \\ 9E_1'' + 10E_2'' \quad (3)$$

$$\Gamma_{T_{12}^H}^{D_{6h}} = 7A_{1g} + 3A_{2g} + 4B_{1g} + 6B_{2g} + 9E_{1g} + 11E_{2g} + \\ 3A_{1u} + 6A_{2u} + 6B_{1u} + 5B_{2u} + 10E_{1u} + 10E_{2u}$$

Each point group D_{nh} correlates with $D_{\infty h}$ as reported for $n = 3, 4, 5,$ and 6 in Table 2, in which the number of symmetry species is included. The horizontal lines separate the irreducible representations relevant for the investigated molecules from the others. Each row shows an equal number of irreducible representations for all molecules. The E_{2g} and E_{2u} start to play a role at D_{4h}. The E_{3g} and E_{3u} start at D_{6h}. This result allows us to correlate the fundamentals row by row. The group theoretical correlation between neighboring D_{nh} point groups was obtained by considering the maximum common symmetry elements of the two groups and the activity of the vibrations.[36] Symmetry lowering from O_h-$H_8Si_8O_{12}$ to D_{4h}-$H_8Si_8O_{12}$ can

therefore be used to correlate all experimental fundamentals of $H_8Si_8O_{12}$ with those of $H_{10}Si_{10}O_{15}$ and to predict the vibrational properties of the yet unknown D_{3h} and D_{6h} species.

Spectra and Normal Coordinate Analysis. The vibrational spectra of $H_8Si_8O_{12}$ and $D_8Si_8O_{12}$ have been interpreted in detail by means of a normal coordinate analysis in terms of symmetry coordinates.[13,14] We now report in Table 3 the results of a normal mode analysis of $H_8Si_8O_{12}$ and $H_{10}Si_{10}O_{15}$ in terms of internal coordinates based on the modified general valence force field described in ref 14. The classification of the vibrations is based on the potential energy distribution (PED) of each normal mode in terms of internal coordinates as proposed by Morino and Kuchitsu.[37] Some of the normal vibrations show similar contributions of ν and δ movements. In these few cases the assignment to a type of vibration based on the greatest contribution to the PED is somewhat arbitrary but still reasonable and useful.

In Figure 2 we compare the experimental IR spectra of H_8-Si_8O_{12} (left) with that of $H_{10}Si_{10}O_{15}$ (most right). We first observe that they bear a similar pattern and a similar intensity distribution. The similarity is easier to recognize in the calculated spectra because they contain no overtone and combination bands. The calculated spectra are in close agreement with the observed frequencies and the relative intensities. Harmonic correction of the experimental Si–H stretching frequencies shifts them close to the calculated values; see ref 14, Table 6. Symmetry lowering and correlation according to Table 2 leads to D_{4h}-$H_8Si_8O_{12}$ and from there to D_{5h}-$H_{10}Si_{10}O_{15}$, in which all IR and Raman active degenerate modes of O_h-H_8-Si_8O_{12} appear as doublets and some of the inactive modes become IR or Raman active. Figure 2 illustrates that all experimentally observed fundamentals can be identified but that some are not resolved and a few are missing. The data in Table 3 show that missing lines have zero or very low intensity and that the splitting of nonresolved bands is smaller than the line widths of the corresponding absorptions. The assignment of the $H_{10}Si_{10}O_{15}$ bands is based on the calculated frequencies and relative IR intensities. It was checked by evaluating the Teller–Redlich product rule[38,39] and by comparing the result to the experimental spectrum of $D_{10}Si_{10}O_{15}$.[33] The calculated splitting of the two O_h-$H_8Si_8O_{12}$ T_{1u} vibrations at 2381 and 1143 cm^{-1} to the D_{5h}-$H_{10}Si_{10}O_{15}$ E_1' plus A_2'' modes is too small to be observed under the applied conditions. The four T_{1u} lines at 881, 569, 481, and 397 cm^{-1} are split by 10, 40, 122, and 48 cm^{-1}, respectively. However, at 569 and 481 cm^{-1} only one absorption was observed because of the low intensity of the A_2'' modes. Out of the four O_h-$H_8Si_8O_{12}$ T_{2u} normal modes two components become IR active in the case of D_{5h}-$H_{10}Si_{10}O_{15}$. They show very weak intensity, in agreement with experiment.

The experimental Raman spectra of $H_8Si_8O_{12}$ (left) and of $H_{10}Si_{10}O_{15}$ (right) in Figure 3 show a similar pattern and a

TABLE 2: Correlation Table of the D_{nh} Subgroups ($n = 3, 4, 5,$ and 6) with Respect to the Point Group $D_{\infty n}$

$D_{\infty h}$	D_{3h}	D_{4h}	D_{5h}	D_{6h}
$A_{1g} \equiv \Sigma_g^+$	$7A_1'$(R)	$7A_{1g}$(R)	$7A_1'$(R)	$7A_{1g}$(R)
$A_{2g} \equiv \Sigma_g^-$	$3A_2'$(in)	$3A_{2g}$(in)	$3A_2'$(in)	$3A_{2g}$(in)
$E_{1g} \equiv \Pi_g$	$9E''$(R)	$9E_g$(R)	$9E_1''$(R)	$9E_{1g}$(R)
$E_{2g} \equiv \Delta_g$	E'	$5B_{1g}$(R) + $6B_{2g}$(R)	$11E_2'$(R)	$11E_{2g}$(R)
$E_{3g} \equiv \Phi_g$	$A_1'' + A_2''$	E_g	E_2''	$4B_{1g}$(in) + $6B_{2g}$(in)
...	...	...	...	...
$A_{1u} \equiv \Sigma_u^+$	$6A_2''$(IR)	$6A_{2u}$(IR)	$6A_2''$(IR)	$6A_{2u}$(IR)
$A_{2u} \equiv \Sigma_u^-$	$3A_1''$(in)	$3A_{1u}$(in)	$3A_1''$(in)	$3A_{1u}$(in)
$E_{1u} \equiv \Pi_u$	$10E'$(IR, R)	$10E_u$(IR)	$10E_1'$(IR)	$10E_{1u}$(IR)
$E_{2u} \equiv \Delta_u$	E''	$6B_{1u}$(in) + $4B_{2u}$(in)	$10E_2''$(in)	$10E_{2u}$(in)
$E_{3u} \equiv \Phi_u$	$A_1' + A_2'$	E_u	E_2'	$6B_{1u}$(in) + $5B_{2u}$(in)
...	...	...	...	...

TABLE 3: IR and Raman Active Fundamentals (cm^{-1}) and Relative IR Intensities (in Parentheses) of $H_8Si_8O_{12}$ and $H_{10}Si_{10}O_{15}$

Left portion — O_h-$H_8Si_8O_{12}$ (with D_{4h}-$H_8Si_8O_{12}$ symmetry):

symmetry	observed	calculated	potential energy distribution (%)	type of vibration	D_{4h} symmetry
A_{1g}(R)	2302	2381	100 R	$\nu(\mathrm{Si{-}H})$	A_{1g}(R)
T_{2g}(R)	2291	2381	100 R	$\nu(\mathrm{Si{-}H})$	B_{2g}(R); E_g(R)
T_{1u}(IR)	2277 (11)	2381 (12)	100 R	$\nu(\mathrm{Si{-}H})$	E_u(IR); A_{2u}(IR)
T_{1g}(in)		1161	98 r	$\nu_{as}(\mathrm{Si{-}O{-}Si})$	E_g(in)
T_{1u}(IR)	1141 (100)	1143 (100)	97 r	$\nu_{as}(\mathrm{Si{-}O{-}Si})$	E_u(IR); A_{2u}(IR)
T_{2g}(R)	1117	1116	97 r	$\nu_{as}(\mathrm{Si{-}O{-}Si})$	E_g(R); B_{2g}(R)
E_g(R)	932	922	77 α + 21 r	$\delta(\mathrm{O{-}Si{-}H})$	A_{1g}(R); B_{1g}(R)
T_{2u}(in)		918	78 α + 20 r	$\delta(\mathrm{O{-}Si{-}H})$	E_u(IR); B_{2u}(in)
T_{2g}(R)	890	894	90 α + 10 r	$\delta(\mathrm{O{-}Si{-}H})$	B_{2g}(R); E_g(R)
T_{1u}(IR)	881 (33)	881 (35)	95 α	$\delta(\mathrm{O{-}Si{-}H})$	A_{2u}(IR); E_u(IR)
T_{1g}(in)		865	99 α	$\delta(\mathrm{O{-}Si{-}H})$	E_g(R); A_{2g}(in)
E_g(R)	697	691	62 r + 23 α + 14 β	$\nu_s(\mathrm{Si{-}O{-}Si})$	A_{1g}(R); B_{1g}(R)
T_{2u}(in)		682	71 r + 20 α	$\nu_s(\mathrm{Si{-}O{-}Si})$	E_u(IR); B_{2u}(in)
T_{2g}(R)	610	613	81 r + 10 α	$\nu_s(\mathrm{Si{-}O{-}Si})$	B_{2g}(R); E_g(R)
A_{1g}(R)	580	576	53 β + 36 α + 11 Φ	$\delta(\mathrm{O{-}Si{-}O})$	A_{1g}(R)
T_{1u}(IR)	566 (1)	569 (0)	45 r + 39 β + 14 α	$\nu_s(\mathrm{Si{-}O{-}Si})$	A_{2u}(IR); E_u(IR)
T_{1u}(IR)	465 (7)	481 (23)	53 r + 23 β + 17 α	$\nu_s(\mathrm{Si{-}O{-}Si})$	E_u(IR); A_{2u}(IR)
A_{1g}(R)	456	446	99 r	$\nu_s(\mathrm{Si{-}O{-}Si})$	A_{1g}(R)
E_g(R)	423	423	78 β + 19 r	$\delta(\mathrm{O{-}Si{-}O})$	B_{1g}(R); A_{1g}(R)
T_{2g}(R)	414	418	46 β + 29 α + 14 r + 11 Φ	$\delta(\mathrm{O{-}Si{-}O})$	B_{2g}(R); E_g(R)
T_{1u}(IR)	399 (19)	397 (30)	79 β + 14 r	$\delta(\mathrm{O{-}Si{-}O})$	A_{2u}(IR); E_u(IR)
T_{1g}(in)		356	89 β	$\delta(\mathrm{O{-}Si{-}O})$	E_g(R); A_{2g}(in)
T_{2u}(in)		303	82 β + 12 r	$\delta(\mathrm{O{-}Si{-}O})$	E_u(IR); B_{2u}(in)
T_{2g}(R)	171	168	86 β	$\delta(\mathrm{O{-}Si{-}O})$	B_{2g}(R); E_g(R)
E_g(R)	84	83	96 Φ	$\delta(\mathrm{Si{-}O{-}Si})$	A_{1g}(R); B_{1g}(R)
T_{2u}(in)		68	92 Φ	$\delta(\mathrm{Si{-}O{-}Si})$	E_u(IR); B_{2u}(in)
A_{2g}(in)		53	100 τ	$\tau_{as}(\mathrm{Si{-}O{-}Si})$	B_{1g}(R)

Right portion — D_{5h}-$H_{10}Si_{10}O_{15}$:

symmetry	observed	calculated	potential energy distribution (%)	type of vibration
A_1'(R)	2293	2381	100 R	$\nu(\mathrm{Si{-}H})$
E_2'(R)	2278	2381	100 R	$\nu(\mathrm{Si{-}H})$
E_1'(R)	2272	2381	100 R	$\nu(\mathrm{Si{-}H})$
E_1'(IR)	2270 (11)	2381 (12)	100 R	$\nu(\mathrm{Si{-}H})$
A_2''(IR)	2270	2381	100 R	$\nu(\mathrm{Si{-}H})$
A_2''(in)		1176	97 s	$\nu_{as}(\mathrm{Si{-}O{-}Si})$
E_1''(R)		1167	65 s + 32 r	$\nu_{as}(\mathrm{Si{-}O{-}Si})$
E_1'(IR)	1147 (100)	1160 (100)	97 s	$\nu_{as}(\mathrm{Si{-}O{-}Si})$
A_2''(IR)	1147	1148	94 r	$\nu_{as}(\mathrm{Si{-}O{-}Si})$
E_1'(R)	1120	1133	63 r + 34 s	$\nu_{as}(\mathrm{Si{-}O{-}Si})$
E_2'(R)	1120	1125	96 s	$\nu_{as}(\mathrm{Si{-}O{-}Si})$
A_1'(R)	939	925	51 α + 25 γ + 14 r	$\delta(\mathrm{O{-}Si{-}H})$
E_2'(R)	926	911	64 γ + 18 α + 12 s	$\delta(\mathrm{O{-}Si{-}H})$
E_1'(IR)	914 (1)	919 (2)	47 α + 31 γ + 12 r	$\delta(\mathrm{O{-}Si{-}H})$
E_2''(in)		902	85 γ + 12 s	$\delta(\mathrm{O{-}Si{-}H})$
E_2'(R)	~902	890	49 γ + 42 α	$\delta(\mathrm{O{-}Si{-}H})$
E_1'(R)	~882	886	62 γ + 32 α	$\delta(\mathrm{O{-}Si{-}H})$
A_2''(IR)	884 (10)	883 (12)	61 α + 33 γ	$\delta(\mathrm{O{-}Si{-}H})$
E_1'(IR)	878 (18)	873 (20)	91 γ	$\delta(\mathrm{O{-}Si{-}H})$
E_1'(IR)		864	68 γ + 31 α	$\delta(\mathrm{O{-}Si{-}H})$
A_2''(IR)		862	99 γ	$\delta(\mathrm{O{-}Si{-}H})$
A_1'(R)	696	707	31 r + 21 s + 16 δ + 15 α + 11 γ	$\nu_s(\mathrm{Si{-}O{-}Si})$
E_2'(R)	696	681	59 s + 14 γ + 12 r + 11 β	$\nu_s(\mathrm{Si{-}O{-}Si})$
E_1'(IR)	680 (1)	694 (2)	34 r + 30 s + 12 α + 10 δ	$\nu_s(\mathrm{Si{-}O{-}Si})$
E_2''(in)		660	79 s + 11 γ	$\nu_s(\mathrm{Si{-}O{-}Si})$
E_2'(R)	598	609	66 s + 21 δ + 10 γ	$\delta(\mathrm{O{-}Si{-}O})$
E_1'(R)	598	605	62 r + 18 β	$\delta(\mathrm{O{-}Si{-}O})$
A_1'(R)	577	590	36 β + 21 γ + 15 δ + 14 α	$\delta(\mathrm{O{-}Si{-}O})$
A_2''(IR)		613 (0)	45 δ + 39 s + 14 γ	$\nu_s(\mathrm{Si{-}O{-}Si})$
E_1'(IR)	559 (7)	573 (9)	43 β + 14 γ + 12 s + 10 α + 10 r	$\nu_s(\mathrm{Si{-}O{-}Si})$
E_1'(IR)	~468 (5)	455 (3)	44 r + 33 s + 15 β	$\nu_s(\mathrm{Si{-}O{-}Si})$
A_2''(IR)		333 (1)	42 s + 40 δ + 16 β	$\nu_s(\mathrm{Si{-}O{-}Si})$
A_1'(R)	453	450	51 r + 18 β + 18 δ + 12 s	$\delta(\mathrm{O{-}Si{-}O})$
E_2'(R)	412	416	63 β + 13 γ + 10 s	$\delta(\mathrm{O{-}Si{-}O})$
A_1'(R)	343	334	52 s + 37 β	$\delta(\mathrm{O{-}Si{-}O})$
E_2'(R)		448	51 β + 18 s + 12 r + 10 γ	$\delta(\mathrm{O{-}Si{-}O})$
E_1'(IR)		428	46 β + 17 α + 12 s + 11 Ψ	$\delta(\mathrm{O{-}Si{-}O})$
A_2''(IR)	437 (5)	459 (17)	43 β + 20 α + 14 s + 10 Ψ	$\delta(\mathrm{O{-}Si{-}O})$
E_1'(IR)	398 (23)	411 (28)	59 β + 24 δ	$\delta(\mathrm{O{-}Si{-}O})$
E_1'(R)		361	49 δ + 29 β + 15 s	$\delta(\mathrm{O{-}Si{-}O})$
A_2''(in)		355	89 β	$\delta(\mathrm{O{-}Si{-}O})$
E_2''(in)		318	42 β + 37 δ + 12 γ	$\delta(\mathrm{O{-}Si{-}O})$
E_1'(IR)		288 (0)	40 β + 37 δ + 18 s	$\delta(\mathrm{O{-}Si{-}O})$
E_2'(R)	202	211	64 δ + 19 β	$\delta(\mathrm{O{-}Si{-}O})$
E_1''(R)	152	148	76 β	$\delta(\mathrm{O{-}Si{-}O})$
A_1'(R)	82	89	58 Φ + 39 Ψ	$\delta(\mathrm{Si{-}O{-}Si})$
E_2'(R)	82	83	88 Ψ	$\delta(\mathrm{Si{-}O{-}Si})$
E_1'(IR)		85 (0)	54 Ψ + 42 Φ	$\delta(\mathrm{Si{-}O{-}Si})$
E_2''(in)		28	86 Ψ + 10 β	$\delta(\mathrm{Si{-}O{-}Si})$
E_2'(R)		4	84 Φ	$\delta(\mathrm{Si{-}O{-}Si})$

Ring-Opening Vibrations of Spherosiloxanes

J. Phys. Chem., Vol. 100, No. 6, 1996 **2039**

Figure 2. Correlation diagram of the IR active fundamentals of $H_8Si_8O_{12}$ (left) and $H_{10}Si_{10}O_{15}$ (right). The transmission IR spectra were measured in CCl_4 with a resolution of 0.5 cm^{-1} and interpolated between 720 and 840 cm^{-1}. The middle part shows the calculated spectra and the correlation of the lines.
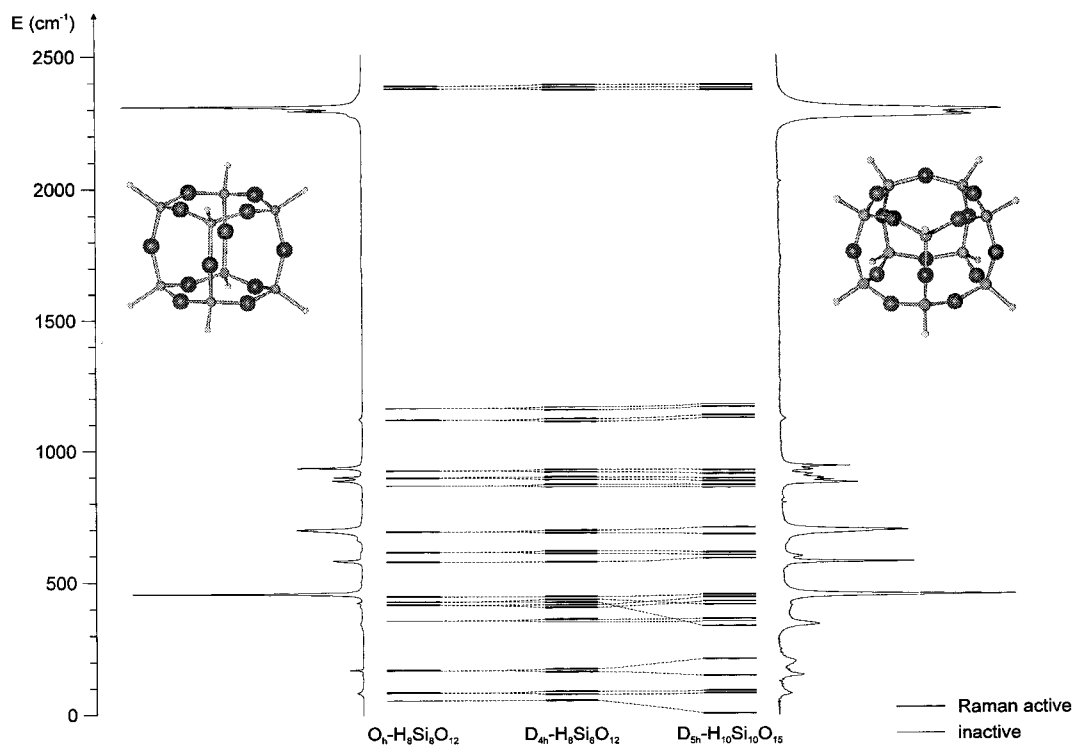
Figure 3. Correlation diagram of the Raman active fundamentals of $H_8Si_8O_{12}$ (left) and $H_{10}Si_{10}O_{15}$ (right). The FT-Raman spectra were measured as crystalline powders with a resolution of 1 cm^{-1}.

similar intensity distribution. The present program version does not allow one to calculate reliable Raman intensities. For this reason we restrict the discussion to the correlation diagram in the middle of Figure 3 and to the data collected in Table 3. We observe that the calculated frequencies agree well with the experimental values. The assignment of the lines of $H_{10}Si_{10}O_{15}$ was checked by evaluating the Teller–Redlich product rule,[38,39] based on the experimental $D_{10}Si_{10}O_{15}$ spectrum.[34] The calculated splitting of the six T_{2g} and the four E_g O_h-$H_8Si_8O_{12}$ modes

is small, in agreement with experiment. The lines at 423 and 168 cm^{-1} are exceptions and are split by 82 and 63 cm^{-1}, respectively, in close agreement with experiment. The inactive O_h-$H_8Si_8O_{12}$ T_{1g} and A_{2g} modes become Raman active for D_{5h}-$H_{10}Si_{10}O_{15}$ but show very weak intensity.

Discussion. The small splitting of most of the degenerate modes, the weak intensity of the lines which become IR or Raman active in the case of D_{5h}-$H_{10}Si_{10}O_{15}$, and the identical force field are the reasons for the close similarity of the

TABLE 4: Group Frequencies (cm⁻¹) of Hydrosilasesquioxanes

	range of frequency		
type of vibration	this work and ref 14	literature[a]	ref
ν(Si−H)	>2200	2260−2100 st	43
ν_{as}(Si−O−Si)	1200−1100	1130−1000 st	40, 41
δ(O−Si−H)	950−850	960−800 m	43
ν_s(Si−O−Si)	750−550	625−480 w	42, 44
δ(O−Si−O)	500−150	580−250	45
δ(Si−O−Si)	<100	120−50	45

[a] st = strong, m = medium, w = weak.

vibrational spectra of $H_8Si_8O_{12}$ and $H_{10}Si_{10}O_{15}$. $H_8Si_8O_{12}$ contains six 4-rings and $H_{10}Si_{10}O_{15}$ five 4- and two 5-rings; see Figure 1. Inspection of the PED analysis reported in Table 3 lays open the nature of the splitting of the degenerate IR and Raman active O_h-$H_8Si_8O_{12}$ modes upon symmetry reduction to D_{4h} and hence in the case of D_{5h}-$H_{10}Si_{10}O_{15}$. We observe that each of them splits into a vibration which may be associated with a 4- and a 5-ring mode with the exceptions of the 418 and 397 cm⁻¹ lines, which split into two 4-ring normal modes.

The vibrations of $H_8Si_8O_{12}$ and $H_{10}Si_{10}O_{15}$ can be divided into the six distinct regions summarized in Table 4 and denoted as ν(Si−H), ν_{as}(Si−O−Si), δ(O−Si−H), ν_s(Si−O−Si), δ(O−Si−O), and δ(Si−O−Si). This means that the concept of group frequencies makes sense, although some normal modes do not fit into this general scheme. The frequency regions are in good agreement with those reported in the literature.[40−45] The symmetric Si−H stretching frequencies are distinctly larger than those of HSi(OSiMe₃)₃ and similar compounds.[46] We have shown that this difference is caused by the differences in the H−Si−O−Si conformation. The cage structure of the spherosiloxanes dictates anti H−Si−O−Si conformation, whereas syn is the stable one for HSi(OSiMe₃)₃.[47] The regions denoted by ν(Si−H), ν_{as}(Si−O−Si), and δ(Si−O−Si) contain normal modes, which may be considered as pure vibrations of the corresponding internal coordinates. However, some of the higher frequency δ(O−Si−H) modes do mix considerably with ν_s(Si−O−Si). In the lower ν_s(Si−O−Si) energy range we observe four vibrations which are primarily of δ(O−Si−O) character, namely, the bands at 576 cm⁻¹ ($H_8Si_8O_{12}$) and 613, 590, and 573 cm⁻¹ ($H_{10}Si_{10}O_{15}$). In the δ(O−Si−O) region five vibrations can be described as being of primarily ν_s(Si−O−Si) character, namely, the bands at 481 and 446 cm⁻¹ ($H_8Si_8O_{12}$) and 455, 450, and 334 cm⁻¹ ($H_{10}S_{10}O_{15}$). The energy of these latter modes correlates with the size of the ring to which they belong. This will be the subject of section V.

IV. Vibrational Spectra of $H_{20}Si_{20}O_{30}$ and $H_{24}Si_{24}O_{36}$

We now extend the discussion to the I_h-$H_{20}Si_{20}O_{30}$ and O_h-$H_{24}Si_{24}O_{36}$ molecules. These cages are parts of many silicates and zeolites[17,20,48] and present models for many of these infinitely extended microporous materials.

Structure and Irreducible Representations. Since I_h-$H_{20}Si_{20}O_{30}$ and O_h-$H_{24}Si_{24}O_{36}$ have not been prepared so far, we apply bond lengths and bond angles based on the following reasoning. Tetrahedral angles at the silicon atoms are assumed. This leads to Si−O−Si angles of 177.1° and 160.5° for $H_{20}Si_{20}O_{30}$ and $H_{24}Si_{24}O_{36}$, respectively. The corresponding Si−O bond lengths were calculated by means of the empirical relation d(Si−O) = 1.59 + [(180 − α)⁴(2.1 × 10⁻⁸)].[4] This leads to 1.59 Å for both molecules. The Si−H bond lengths reported in Table 1 are used. The vibrational degrees of freedom for the I_h-$H_{20}Si_{20}O_{30}$ and the O_h-$H_{24}Si_{24}O_{36}$ are divided among the irreducible representations of the corresponding point groups

as follows:

I_h-$H_{20}Si_{20}O_{30}$:

$$\Gamma_{vib} = 3A_g + 3T_{1g} + 4T_{2g} + 7G_g + 10H_g + 6T_{1u} + 7T_{2u} + 7G_u + 7H_u \quad (4)$$

O_h-$H_{24}Si_{24}O_{36}$:

$$\Gamma_{vib} = 7A_{1g} + 6A_{2g} + 13E_g + 13T_{1g} + 15T_{2g} + 3A_{1u} + 5A_{2u} + 8E_u + 17T_{1u} + 16T_{2u} \quad (5)$$

From the selection rules follows that six $T_{1u} \leftarrow A_g$ transitions and 17 $T_{1u} \leftarrow A_{1g}$ transitions are IR active for $H_{20}Si_{20}O_{30}$ and $H_{24}Si_{24}O_{36}$, respectively. The three $A_g \leftarrow A_g$ and the 10 $H_g \leftarrow A_g$ transitions are Raman active in the case of $H_{20}Si_{20}O_{30}$, whereas seven $A_{1g} \leftarrow A_{1g}$, 13 $E_g \leftarrow A_{1g}$, and 15 $T_{2g} \leftarrow A_{1g}$ transitions are Raman active for $H_{24}Si_{24}O_{36}$.

Spectra and Normal Coordinate Analysis. The calculated frequencies and the PED results are collected in Tables 5S and 6S, and the spectra are shown in Figures 4 and 5. The six IR active modes of $H_{20}Si_{20}O_{30}$ can be compared directly with the six IR active modes of $H_8Si_8O_{12}$. We observe in Figure 4 (left) that the three highest energy absorptions are almost equal in frequency and in relative intensity, while the 569, 481, and 397 cm⁻¹ O_h-$H_8Si_8O_{12}$ lines shift to 637, 284, and 439 cm⁻¹, respectively, and change in intensity. The PED analysis indicates that if a δ(O−Si−O) band increases in energy, its character is enhanced. The reverse is observed for ν_s(Si−O−Si) vibrations. The intensity changes of these lines correlate with the fact that symmetric Si−O−Si stretching vibrations show in general low infrared intensity, whereas δ(O−Si−O) movements give considerable IR absorptions.[43] On the right side of Figure 4 we compare the spectra of $H_8Si_8O_{12}$, $H_{10}Si_{10}O_{15}$, and $H_{24}Si_{24}O_{36}$. The spectra of the two latter ones are very similar. From the potential energy distribution analysis we find that each of the O_h-$H_8Si_8O_{12}$ T_{1u} IR lines at 1143, 881, 569, and 481 cm⁻¹ split into a 4- and 6-ring vibration in the case of the O_h-$H_{24}Si_{24}O_{36}$. The four T_{2u} O_h-$H_8Si_8O_{12}$ normal modes at 918, 682, 303, and 68 cm⁻¹ correlate with the T_{1u} 4-ring vibration at 894 cm⁻¹ and the T_{1u} 6-ring vibrations at 726, 309, and 85 cm⁻¹ of O_h-$H_{24}Si_{24}O_{36}$.

The Raman spectrum of $H_{20}Si_{20}O_{30}$ compares in a similar way to that of $H_8Si_8O_{12}$. Both show the same number of Raman active vibrations, three totally symmetric and 10 non-totally symmetric. The correlation of the energy levels is shown in Figure 5 (left). The broken lines connect modes of the same type. The ring-opening vibrations discussed in the next section are marked with the label RO. This correlation shows that for I_h-$H_{20}Si_{20}O_{30}$ out of the 13 Raman active lines of O_h-$H_8Si_8O_{12}$ only the three at 576, 446, and 418 cm⁻¹ shift considerably, namely, to 645, 251, and 336 cm⁻¹, respectively. This leads to very similar spectra for $H_{20}Si_{20}O_{30}$ and $H_8Si_8O_{12}$. The $H_8Si_8O_{12}$ via $H_{10}Si_{10}O_{15}$ to $H_{24}Si_{24}O_{36}$ correlation is more difficult due to the considerable increase of the number of Raman active modes from 13 to 27 to 35 lines, respectively. However, the number of totally symmetric normal modes remains constant from D_{4h}-$H_8Si_8O_{12}$ to D_{5h}-$H_{10}Si_{10}O_{15}$ to O_h-$H_{24}Si_{24}O_{36}$, and unambiguous correlation is possible. It is indicated by broken lines in Figure 5 (right) and shows that only the 423 cm⁻¹ line of $H_8Si_8O_{12}$ shifts considerably, namely, to 334 cm⁻¹ (D_{5h}-$H_{10}Si_{10}O_{15}$) and to 214 cm⁻¹ in the case of O_h-$H_{24}Si_{24}O_{36}$. This correlation corresponds to the transition of a 4- to a 5-ring and finally to a 6-ring vibration.

Ring-Opening Vibrations of Spherosiloxanes

J. Phys. Chem., Vol. 100, No. 6, 1996 **2041**
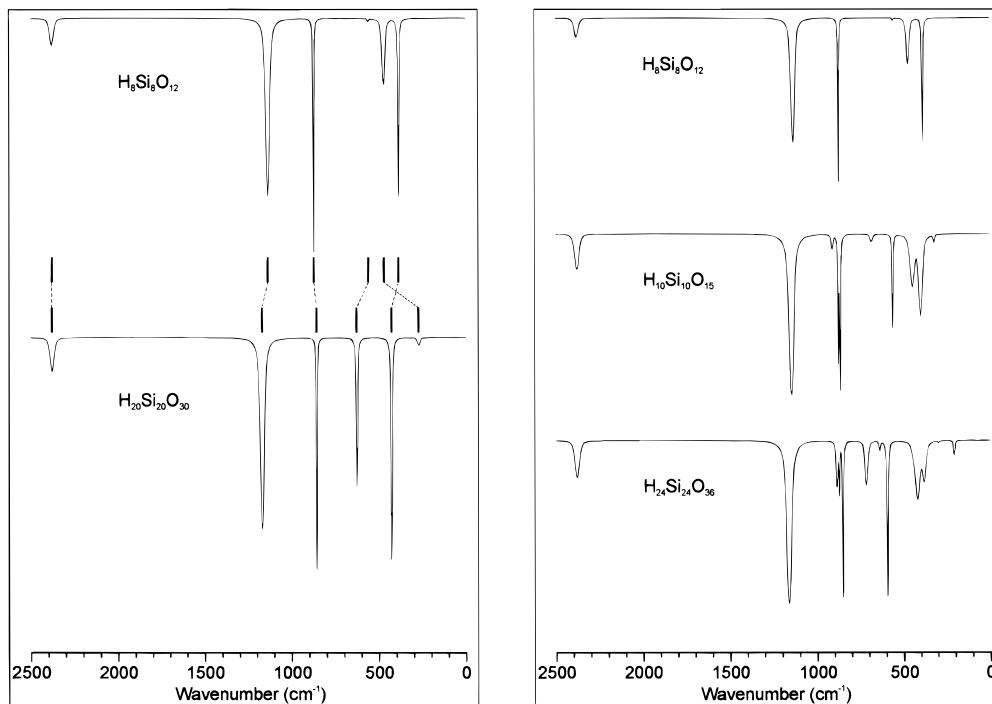
Figure 4. Calculated transmission IR spectra of $H_8Si_8O_{12}$ and $H_{20}Si_{20}O_{30}$ (left) and of $H_8Si_8O_{12}$, $H_{10}Si_{10}O_{15}$, and $H_{24}Si_{24}O_{36}$ (right).
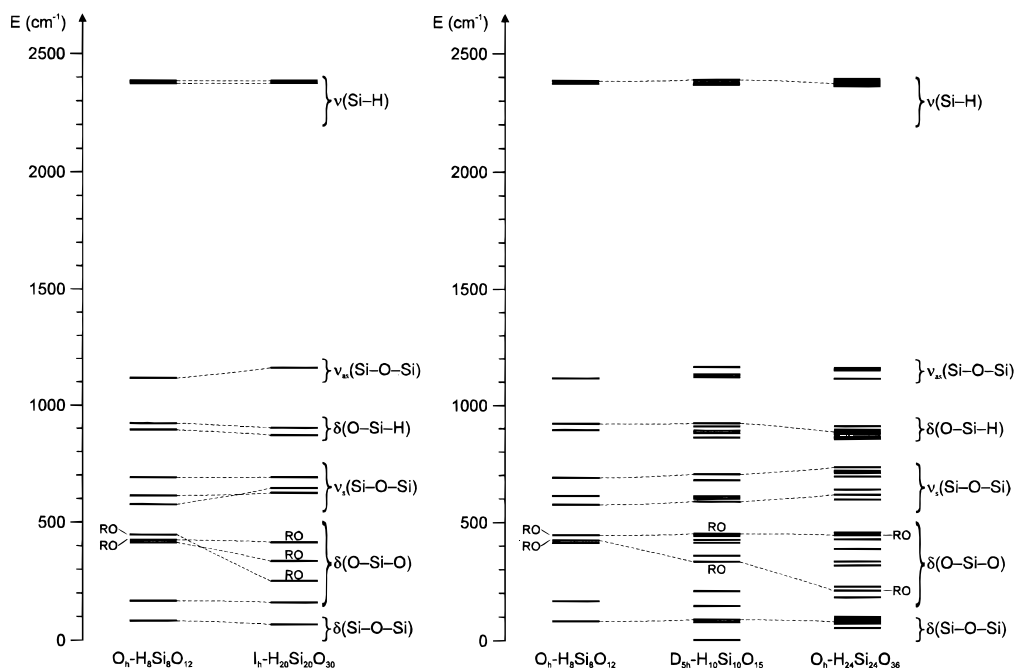
Figure 5. Calculated Raman lines of $H_8Si_8O_{12}$ and $H_{20}Si_{20}O_{30}$ (left) and of $H_8Si_8O_{12}$, $H_{10}Si_{10}O_{15}$, and $H_{24}Si_{24}O_{36}$ (right). RO = ring-opening vibrations.

Discussion. $H_8Si_8O_{12}$ and $H_{20}Si_{20}O_{30}$ are composed of 4- and 5-rings, respectively. Both molecules have an equal number of IR and Raman active fundamentals. This enables us to correlate the normal modes associated with 4-rings with those associated with 5-rings in a direct way. The calculated spectra of $H_8Si_8O_{12}$, $H_{10}Si_{10}O_{15}$, and $H_{24}Si_{24}O_{36}$ shown at the right side of Figures 4 and 5 give a clear qualitative picture of the development as the size and complexity of the molecules increase. In general, more bands appear in each region denoted in Table 4 when the molecules become larger, as expected. The infrared bands show in general an intensity enhancement in the $\nu_s(Si-O-Si)$ and $\delta(O-Si-O)$ regions. As in the previous section, we find that the concept of group frequencies is

applicable and makes good sense for $H_{20}Si_{20}O_{30}$ and $H_{24}Si_{24}O_{36}$. However, some vibrations do not fit into the general scheme of Table 4. We observe five $\delta(O-Si-O)$ in the $\nu_s(Si-O-Si)$ region, namely, at 645 and 637 cm^{-1} ($H_{20}Si_{20}O_{30}$) and 620, 605, and 599 cm^{-1} ($H_{24}Si_{24}O_{36}$), while five $\nu_s(Si-O-Si)$ appear in the $\delta(O-Si-O)$ region, namely, at 336, 284, and 251 cm^{-1} ($H_{20}Si_{20}O_{30}$) and at 219 and 214 cm^{-1} ($H_{24}Si_{24}O_{36}$). The energy of the latter ones correlates with the size of the ring to which they belong, as will be shown in the next section.

V. Ring-Opening Vibrations of Spherosiloxanes

We define the ring-opening vibrations as normal modes in which all Si$-$O stretching and/or O$-$Si$-$O angle bending

SCHEME 5: Set of Equivalent Internal Coordinates Defining the Ring-Opening Vibrations of $H_8Si_8O_{12}$
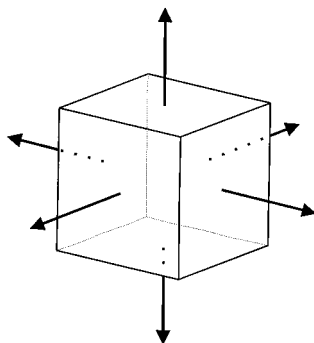
displacements of the considered ring are in phase. To determine the symmetry species of these modes, we introduced new sets of internal coordinates as illustrated in Scheme 5 for the hexahedron which represents the Si_8 cage of $H_8Si_8O_{12}$. Each arrow is a representation of the corresponding 4-ring perpendicular to it. Therefore, the displacements of the new coordinates may be considered as a breathing motion of the ring. This leads to the following irreducible representations of these vibrations for the different cages.

six 4-rings ($H_8Si_8O_{12}$):
$$\Gamma_{RO}^{4R} = A_{1g} + E_g + T_{1u}$$

five 4- and two 5-rings ($H_{10}Si_{10}O_{15}$):
$$\Gamma_{RO}^{4R} = A_1' + E_1' + E_2'$$
$$\Gamma_{RO}^{5R} = A_1' + A_2'' \qquad (6)$$

12 5-rings ($H_{20}Si_{20}O_{30}$):
$$\Gamma_{RO}^{5R} = A_g + H_g + T_{1u} + T_{2u}$$

six 4- and eight 6-rings ($H_{24}Si_{24}O_{36}$):
$$\Gamma_{RO}^{4R} = A_{1g} + E_g + T_{1u}$$
$$\Gamma_{RO}^{6R} = A_{1g} + T_{2g} + A_{2u} + T_{1u}$$

To apply this geometrical concept to the spherosiloxane cages, we must multiply each symmetry species with the number of appearance, which may be different from that of the polyhedron, because of the oxygen bridges. We have done this by visual representation of normal modes on a computer screen, using the computer program MOBY,[49] and analyzing all normal modes of the symmetry species in eq 6. The result of this analysis is given in eq 7.

$H_8Si_8O_{12}$:
$$\Gamma_{RO}^{4R} = A_{1g} + E_g + 2T_{1u}$$

$H_{10}Si_{10}O_{15}$:
$$\Gamma_{RO}^{4R} = A_1' + 2E_1' + 2E_2'$$
$$\Gamma_{RO}^{5R} = A_1' + A_2'' \qquad (7)$$

$H_{20}Si_{20}O_{30}$:
$$\Gamma_{RO}^{5R} = A_g + 2H_g + 2T_{1u} + 2T_{2u}$$

$H_{24}Si_{24}O_{36}$:
$$\Gamma_{RO}^{4R} = A_{1g} + 2E_g + 2T_{1u}$$
$$\Gamma_{RO}^{6R} = A_{1g} + 2T_{2g} + A_{2u} + 2T_{1u}$$

In Figure 6 the 11 IR active and in Figure 7 the 15 Raman active ring-opening normal modes of the investigated hydrosilasesquioxanes are illustrated as projections. The three inactive ring-opening modes are not shown. Figures 6 and 7 are arranged such that the vibrational energy decreases from left to
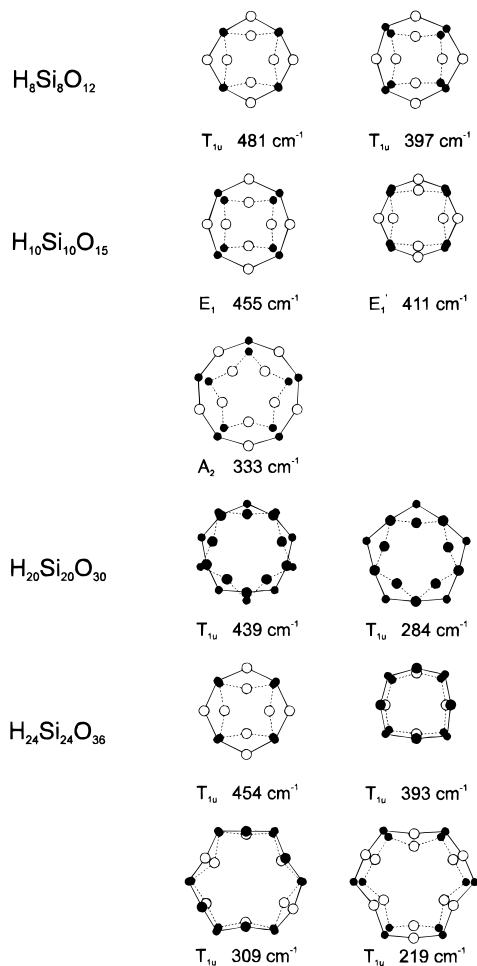
Figure 6. Projection of the IR active ring-opening vibrations of hydrosilasesquioxanes along the rotational axes perpendicular to the ring. The front rings (straight lines) and the back rings (dashed lines) represent the positions with maximum potential energy. The amplitudes are magnified by a factor of 10. Si = solid circles; O = open circles.

right. The filled circles correspond to the Si atoms, and the open circles, to oxygen atoms. We show the maximum potential energy geometries with amplitudes multiplied by a factor of 10. Because of the antisymmetric nature of the IR ring-opening vibrations in Figure 6, the top and the bottom ring openings are out of phase by 180°. The projection illustrates the maximum (solid lines) and the minimum (dashed lines) pore size. Since the top and the bottom Raman active pore opening vibrations are in phase, minimum and maximum positions are connected by solid lines.

Discussion. The energy regions of the 4-, 5-, and 6-ring-opening vibrations decrease from 490−390 to 440−250 to 340−210 cm^{-1}, respectively. The energy of the 5-ring- and 6-ring-opening vibrations depends on their character. The PED results in Tables 3, 5S, and 6S show that an increase in stretching character of a ring-opening mode correlates with a decrease in vibrational energy, but this is less pronounced in the case of the 4-ring modes. The totally symmetric vibrations show predominantly stretching character with the exception of the line at 451 cm^{-1} for $H_{24}Si_{24}O_{36}$. They occur in specific regions, namely, at 460−440 cm^{-1} for the 4-ring, at 340−250 cm^{-1} for the 5-ring, and at 220−210 cm^{-1} for the 6-ring.

In a previous study of the vibrations of zeolite A,[14] we discussed the four frequencies at 476, 288, 271, and 214 cm^{-1}, which are primarily of symmetric T−O−T stretching character and fall into the δ(O−T−O) region. We assigned them to a D4R breathing mode, two 6-ring vibrations of the sodalite cage,

Ring-Opening Vibrations of Spherosiloxanes

J. Phys. Chem., Vol. 100, No. 6, 1996 **2043**
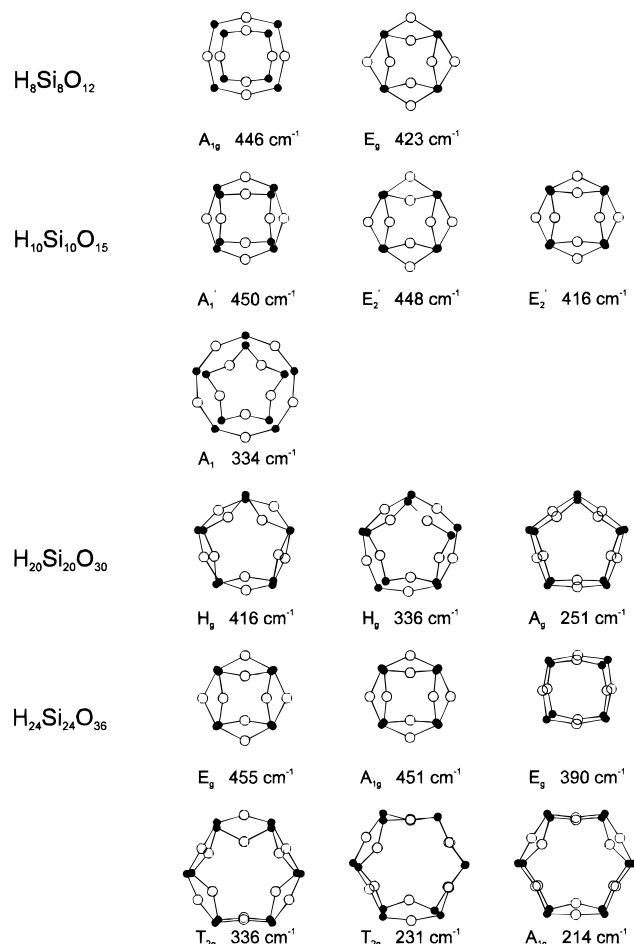
Figure 7. Projection of the Raman active ring-opening vibrations of hydrosilasesquioxanes along the rotational axes perpendicular to the ring. The two rings represent the positions of the front ring with maximum potential energy. The amplitudes are magnified by a factor of 10. Si = solid circles; O = open circles.

and a 8-ring pore-opening vibration of the α-cage, respectively. In this study we observed 10 vibrations which do not fit into the group frequencies in Table 4, namely, the modes at 481 and 446 cm^{-1} ($H_8Si_8O_{12}$), at 455, 450, and 334 cm^{-1} (H_{10}-$Si_{10}O_{15}$), at 336, 284, and 251 cm^{-1} ($H_{20}Si_{20}O_{30}$), and at 219 and 214 cm^{-1} ($H_{24}Si_{24}O_{36}$). All of them can be identified as ring-opening vibrations.

We now compare the ring-opening modes of the investigated hydrosilasesquioxanes with the available literature data on pore-opening vibrations of zeolites. Flanigen et al. observed two bands at 378 and 260 cm^{-1} in the infrared spectrum of zeolite A, which they assigned to pore-opening vibrations.[50] No and co-workers assigned them to normal modes of the 6-rings and to the pore-opening vibration of the double 4-rings, respectively, on the basis of a pseudolattice study of the D4R.[24b] Our analysis of the ring-opening vibrations shows, however, that the reverse assignment might be correct. Dutta et al. reported two lines at 410 and 337 cm^{-1} in the Raman spectrum of zeolite A, which are assigned to the motion of oxygen atoms of the double 4-rings.[21] In a recent local-mode analysis of zeolite A two local modes at 446 and 442 cm^{-1} were attributed to the D4R breathing vibrations.[26] This agrees well with the region of the four-membered ring-opening vibrations of hydrosilasesquioxanes. Bougeard and co-workers assigned the observed bands at 285 and 108 cm^{-1} to the pore opening of the double 4-rings and the breathing motion of the 8-ring (window), respectively, on the basis of a molecular dynamics study of window fluctuations in zeolite A.[51] This can be compared to the decreasing

frequency of the ring-opening vibration from ∼440 (4-ring), to ∼350 (5-ring), and to ∼290 cm^{-1} (6-ring) we have observed. The 5-rings in the ZSM-5 framework cause a shift of the prominent Raman band from ∼490 to ∼390 cm^{-1}.[23] This compares well to our observation that the 446 cm^{-1} double 4-ring breathing mode of $H_8Si_8O_{12}$ shifts to 334 cm^{-1} in H_{10}-$Si_{10}O_{15}$.

Supporting Information Available: Structures and internal coordinates of $H_8Si_8O_{12}$, $H_{10}Si_{10}O_{15}$, $H_{20}Si_{20}O_{30}$, and $H_{24}Si_{24}O_{36}$ (Schemes 3S and 4S) and calculated IR and Raman active fundamentals and relative IR intensities of $H_{20}Si_{20}O_{30}$ and H_{24}-$Si_{24}O_{36}$ (Tables 5S and 6S) (5 pages). Ordering information is given on any current masthead page.

References and Notes

(1) Larsson, K. *Ark. Kemi* **1960**, *16*, 215.
(2) Auf der Heyde, T. P. E.; Bürgi, H.-B.; Bürgy, H.; Törnroos, K. W. *Chimia* **1991**, *45*, 38.
(3) Törnroos, K. W. *Acta Crystallogr.* **1994**, *C50*, 1646.
(4) Bürgi, H.-B.; Bürgy, H.; Calzaferri, G.; Törnroos, K. W. *Inorg. Chem.* **1993**, *32*, 4914.
(5) Törnroos, K. W.; Bürgi, H.-B.; Calzaferri, G.; Bürgy, H. *Acta Crystallogr.* **1994**, *B51*, 155.
(6) Agaskar, P. A.; Day, V. W.; Klemperer, W. G. *J. Am. Chem. Soc.* **1987**, *109*, 5554.
(7) (a) Lee, S.; Makan, S.; Banazak Holl, M. M.; McFeely, F. R. *J. Am. Chem. Soc.* **1994**, *116*, 11819. (b) Nyman, M. D.; Desu, S. B.; Peng, C. H. *Chem. Mater.* **1993**, *5*, 1636.
(8) (a) Calzaferri, G. *Proceedings of Tailor-made Silicon-Oxygen Compounds*; Jutzi, P., Ed.; Bielefeld Sept 3−5, 1995, in press. (b) Calzaferri, G.; Imhof, R.; Törnroos, K. W. *J. Chem. Soc., Dalton Trans.* **1994**, 3123. (c) Calzaferri, G.; Imhof, R.; Törnroos, K. W. *J. Chem. Soc., Dalton Trans.* **1993**, 3741. (d) Calzaferri, G.; Imhof, R. *J. Chem. Soc., Dalton Trans.* **1992**, 3391. (e) Calzaferri, G.; Herren, D.; Imhof, R. *Helv. Chim. Acta* **1991**, *74*, 1278.
(9) (a) Hendan, B. J.; Marsmann, H. C. *J. Organomet. Chem.* **1994**, *483*, 33. (b) Jutzi, P.; Batz, C.; Mutluay, A. *Z. Naturforsch.* **1994**, *49b*, 1689. (c) Morán, M.; Casado, C. M.; Cuadrado, I.; Losada, J. *Organometallics* **1993**, *12*, 4327. (d) Herren, D.; Bürgy, H.; Calzaferri, G. *Helv. Chim. Acta* **1991**, *74*, 24. (e) Bürgy, H.; Calzaferri, G. *Helv. Chim. Acta* **1990**, *73*, 698.
(10) (a) Calzaferri, G.; Hoffmann, R. *J. Chem. Soc., Dalton Trans.* **1991**, 917. (b) Earley, C. W. *Inorg. Chem.* **1992**, *31*, 1250.
(11) (a) Feher, F. J.; Weller, K. J.; Schwab, J. J. *Organometallics* **1995**, *14*, 2009. (b) Lichtenhan, J. D. *Comments Inorg. Chem.* **1995**, *17*, 115. (c) Hoebbel, D.; Pitsch, I.; Heidemann, D. *Z. Anorg. Allg. Chem.* **1991**, *592*, 207. (d) Day, V. M.; Klemperer, W. G.; Mainz, V. V.; Millar, D. M. *J. Am. Chem. Soc.* **1985**, *107*, 8262.
(12) Sasamori, S.; Okaue, Y.; Isobe, T.; Matsuda, Y. *Science* **1994**, *265*, 1691.
(13) (a) Bärtsch, M.; Bornhauser, P.; Calzaferri, G. *SPIE* **1992**, *1575*, 588. (b) Bärtsch, M.; Bornhauser, P.; Bürgy, H.; Calzaferri, G. *Spectrochim. Acta* **1991**, *47A*, 1627. (c) Bornhauser, P.; Calzaferri, G. *Spectrochim. Acta* **1990**, *46A*, 1045.
(14) Bärtsch, M.; Bornhauser, P.; Calzaferri, G.; Imhof, R. *J. Phys. Chem.* **1994**, *98*, 2817.
(15) Calzaferri, G.; Marcolli, C.; Tomkinson, J. *ISIS Exp. Rep.* **1995**.
(16) Bärtsch, M.; Bornhauser, P.; Calzaferri, G.; Imhof, R. *Vib. Spectrosc.* **1995**, *8*, 305.
(17) Meier, W. M.; Olson, D. H. *Atlas of Zeolite Structure Types*; Butterworth: Stoneham, MA, 1988.
(18) Bieniok, A. M.; Bürgi, H.-B. *J. Phys. Chem.* **1994**, *98*, 10735.
(19) Beagley, B.; Titiloye, J. O. *Struct. Chem.* **1992**, *3*, 429.
(20) Gerke, H.; Gies, H. *Z. Kristallogr.* **1984**, *166*, 11.
(21) Dutta, P. K.; del Barco, B. *J. Phys. Chem.* **1988**, *92*, 354.
(22) Dutta, P. K.; Shieh, D. C.; Puri, M. *Zeolites* **1988**, *8*, 306.
(23) Dutta, P. K.; Rao, K. M.; Park, J. Y. *J. Phys. Chem.* **1991**, *95*, 6654.

(24) (a) Blackwell, C. S. *J. Phys. Chem.* **1979**, *83*, 3251, 3257. (b) No, K. T.; Bae, D. H.; Jhon, M. S. *J. Phys. Chem.* **1986**, *90*, 1772. (c) de Man, A. J. M.; van Santen, R. A. *Zeolites* **1992**, *12*, 269. (d) Geidel, E.; Boehlig, H.; Peuker, C.; Pilz, W. *Z. Chem.* **1988**, *28*, 155.

(25) Creighton, J. A.; Deckman, H. W.; Newsam, J. M. *J. Phys. Chem.* **1994**, *98*, 448.

(26) Iyer, K. A.; Singer, S. J. *J. Phys. Chem.* **1994**, *98*, 12670, 12679.

(27) Deem, M. W.; Newsam, J. M.; Creighton, J. A. *J. Am. Chem. Soc.* **1992**, *114*, 7198.

(28) Wilson, E. B., Jr.; Decius, J. C.; Cross, P. C. *Molecular Vibrations*; McGraw-Hill Book Co., Inc.: New York, 1955.

(29) McIntosh, D. F.; Peterson, M. R. *General Vibrational Analysis System*; QCPE Program No. QCMP067, 1988.

(30) Calzaferri, G.; Brändle, M. QCMP No. 116, *QCPE Bulletin*, **1992**, *12* (4), update May 1993.

(31) Bürgy, H.; Calzaferri, G. *J. Chromatogr.* **1990**, *507*, 481.

(32) Agaskar, P. A. *Inorg. Chem.* **1991**, *30*, 2707.

(33) Imhof, R. Ph.D. Thesis, Universität Bern, 1994.

(34) Bärtsch, M. Ph.D. Thesis, Universität Bern, 1993.

(35) Salthouse, J. A.; Ware, M. J. *Point Group Character Tables and Related Data*; Cambridge University Press: London, 1972.

(36) Bornhauser, P. Ph.D. Thesis, Universität Bern, 1992.

(37) Morino, Y.; Kuchitsu, K. *J. Chem. Phys.* **1952**, *20*, 1809.

(38) Teller, E. quoted by Angus, W. R.; et al. *J. Chem. Soc.* **1936**, 971.

(39) Redlich, O. *Z. Physl. Chem. (B)* **1935**, *28*, 371.

(40) Colthup, N. B.; Daly, L. H.; Wiberley, S. E. *Introduction to Infrared and Raman Spectroscopy*, 3rd ed.; Academic Press, Inc.: London, 1990.

(41) Bellamy, L. J. *The Infra-red Spectra of Complex Molecules*, 3rd ed.; Chapman and Hall Ltd.: London, 1975.

(42) Kriegsmann, H. *Z. Elektrochem. Ber. Bunsen-Ges. Phys. Chem.* **1961**, *65*, 336, 342.

(43) Smith, A. L. *Spectrochim. Acta* **1960**, *16*, 87.

(44) Smith, A. L. *Spectrochim. Acta* **1963**, *19*, 849.

(45) Geidel, E.; Bauer, F.; Böhlig, H.; Kudra, M. *Acta Chim. Hung.*, in press.

(46) McKean, D. C.; Torto, I. *Spectrochim. Acta* **1993**, *49A*, 1095.

(47) Bärtsch, M.; Calzaferri, G.; Marcolli, C. *Res. Chem. Intermed.* **1995**, *6*, 577.

(48) (a) Smith, J. V. *Chem. Rev.* **1988**, *88*, 149. (b) Breck, D. W. *Zeolite Molecular Sieves*; John Wiley & Sons, Inc.: New York, 1974.

(49) Höweler, U. *MOBY*, Molecular Modelling on the PC, Version 1.6F; Springer Verlag: Berlin, 1993.

(50) Flanigen, E. M.; Khatami, H.; Szymanski, H. A. *Adv. Chem. Ser.* **1971**, *101*, 201.

(51) (a) Brémard, C.; Bougeard, D. *Adv. Mater.* **1995**, *7*, 10. (b) Smirnov, K. S.; Bougeard, D. *J. Mol. Struct.* **1995**, *348*, 155. (c) Smirnov, K. S.; Le Maire, M.; Brémard, C.; Bougeard, D. *Chem. Phys.* **1994**, *179*, 445. (d) Ermoshin, V. A.; Smirnov, K. S.; Bougeard, D. *Chem. Phys.*, in press.

JP952198T